A&A 641, L9 (2020)
https://doi.org/10.1051/0004-6361/202039231

Astronomy & Astrophysics

LETTER TO THE EDITOR

Interstellar nitrile anions: Detection of C_3N^- and C_5N^- in TMC-1⋆

J. Cernicharo[1], N. Marcelino[1], J. R. Pardo[1], M. Agúndez[1], B. Tercero[2,3], P. de Vicente[2], C. Cabezas[1], and C. Bermúdez[1]

[1] Grupo de Astrofísica Molecular, Instituto de Física Fundamental (IFF-CSIC), C/ Serrano 121, 28006 Madrid, Spain
e-mail: jose.cernicharo@csic.es
[2] Centro de Desarrollos Tecnológicos, Observatorio de Yebes (IGN), 19141 Yebes, Guadalajara, Spain
[3] Observatorio Astronómico Nacional (IGN), C/ Alfonso XII, 3, 28014 Madrid, Spain

Received 21 August 2020 / Accepted 30 August 2020

ABSTRACT

We report on the first detection of C_3N^- and C_5N^- towards the cold dark core TMC-1 in the Taurus region, using the Yebes 40 m telescope. The observed C_3N/C_3N^- and C_5N/C_5N^- abundance ratios are ∼140 and ∼2, respectively; that is similar to those found in the circumstellar envelope of the carbon-rich star IRC +10216. Although the formation mechanisms for the neutrals are different in interstellar (ion-neutral reactions) and circumstellar clouds (photodissociation and radical-neutral reactions), the similarity of the C_3N/C_3N^- and C_5N/C_5N^- abundance ratios strongly suggests a common chemical path for the formation of these anions in interstellar and circumstellar clouds. We discuss the role of radiative electronic attachment, reactions between N atoms and carbon chain anions C_n^-, and that of H^- reactions with HC_3N and HC_5N as possible routes to form C_nN^-. The detection of C_5N^- in TMC-1 gives strong support for assigning to this anion the lines found in IRC +10216, as it excludes the possibility of a metal-bearing species, or a vibrationally excited state. New sets of rotational parameters have been derived from the observed frequencies in TMC-1 and IRC +10216 for C_5N^- and the neutral radical C_5N.

Key words. astrochemistry – ISM: lines and bands – ISM: molecules – ISM: individual objects: TMC-1 – molecular data

1. Introduction

The importance of anions in the chemistry of interstellar clouds was analyzed in the early years of astrochemistry by Dalgarno & McCray (1973). The presence of carbon chain negative ions in space was predicted on the ground that electron radiative attachment is efficient for molecules with large electron affinities and dense vibrational spectra (Sarre 1980; Herbst 1981).

The first anion detected in space, C_6H^-, was observed towards TMC-1 (McCarthy et al. 2006). Lines from this species were already reported as unidentified features in the line survey of IRC +10216 performed with the Nobeyama 45 m telescope by Kawaguchi et al. (1995). Their assignation to C_6H^- was not possible until the laboratory observations of McCarthy et al. (2006) became available. Nevertheless, Aoki (2000) suggested that the carrier of these lines was C_6H^- from ab initio calculations. The laboratory and space detection of this species prompted attention to the abundance of hydrocarbon anions in interstellar and circumstellar clouds. C_4H^- was first discovered in the circumstellar cloud IRC +10216 by Cernicharo et al. (2007) and then in the interstellar clouds L1527 and TMC-1 (Sakai et al. 2008; Agúndez et al. 2008a; Cordiner et al. 2013). C_6H^- was also detected towards other interstellar sources (Sakai et al. 2007; Gupta et al. 2009; Cordiner et al. 2011, 2013). Following the observation of C_8H^- in the laboratory (Gupta et al. 2007) this anion was found in TMC-1 (Brünken et al. 2007) and IRC +10216 (Kawaguchi et al. 2007; Remijan et al. 2007).

The nitrile anions CN^-, C_3N^- and C_5N^- were first detected in the circumstellar envelope of the carbon-rich star IRC +10216 (Agúndez et al. 2010; Thaddeus et al. 2008; Cernicharo et al. 2008). While accurate laboratory frequencies were available for CN^- and C_3N^- (Gottlieb et al. 2007; Thaddeus et al. 2008; Amano 2008), the assignment of C_5N^- was based on the coincidence of the observed rotational constants with ab initio calculations by Botschwina & Oswald (2008) and Aoki (2000). Although this species is the best candidate for this identification, the lack of precise laboratory frequencies prevents us from ruling out other species involving metals, which are present in IRC +10216. For example, MgC_3N and MgC_4H have been recently detected in IRC +10216 based on ab initio calculations (Cernicharo et al. 2019) and they have rotational constants B just a few megahertz below that of C_5N^-. Moreover, there is controversy about the formation of C_nN^- anions through radiative electron attachment to C_nN radicals, for which calculated rate constants differ by orders of magnitude (Walsh et al. 2009; Khamesian et al. 2016; Millar et al. 2017). Hence, the detection of these anions in cold dark clouds and the determination of their abundances are an important step forward in understanding their chemistry in different astronomical environments.

In this Letter we present the detection of C_3N^- and C_5N^- in the cold dark core TMC-1. This is the first time nitrile anions are observed in the interstellar medium. The C_3N/C_3N^- and

⋆ Based on observations carried out with the Yebes 40 m telescope (projects 19A003, 19A010, and 20A014) and the Institut de Radioastronomie Millimétrique (IRAM) 30 m telescope. The 40 m radiotelescope at Yebes Observatory is operated by the Spanish Geographic Institute (IGN, Ministerio de Transportes, Movilidad y Agenda Urbana). IRAM is supported by INSU/CNRS (France), MPG (Germany), and IGN (Spain).

C_5N/C_5N^- abundance ratios derived are discussed within the frame of a chemical model of a cold dense cloud.

2. Observations

The Q-band (31.0−50.3 GHz) observations of TMC-1 ($\alpha_{2000} = 4^h41^m42.0^s$, $\delta_{2000} = 25°41'27.6''$) were carried out during the winter 2019/2020 with the 40 m radio telescope of the Yebes observatory (IGN, Spain), hereafter Yebes 40 m. Observations of IRC +10216 in the same frequency band were performed in spring 2019 and have been previously described by Cernicharo et al. (2019) and Pardo et al. (2020). New receivers were built within the Nanocosmos project[1] and installed at the telescope (Tercero 2020). They were used for the observations presented in this work. The Q-band receiver consists of two HEMT cold amplifiers covering the 31.0−50.3 GHz band with horizontal and vertical polarisations. Receiver temperatures vary from 22 K at 32 GHz to 42 K at 50 GHz. The backends are 16 × 2.5 GHz fast Fourier transform spectrometers (FFTS) with a spectral resolution of 38.1 kHz providing the whole coverage of the Q band in both polarisations. The main beam efficiency varies from 0.6 at 32 GHz to 0.43 at 50 GHz. Pointing corrections obtained by observing strong nearby quasars and were always within 2−3″.

For IRC +10216 the observing mode was position switching with an off position at 300″ in azimuth. The final spectra were smoothed to a resolution of 0.15 MHz, that is a velocity resolution of ≈1.5 and 0.9 km s^{-1} at 31 and 50 GHz, respectively. The sensitivity of the final spectra varies between 0.4 mK and 1 mK per 0.15 MHz channel across the Q band, which is a factor of ≈10 better than previous observations in the same frequency range with the Nobeyama 45 m telescope taken with a spectral resolution of 0.5−0.625 MHz (Kawaguchi et al. 1995).

The TMC-1 Q-band observations were performed using the frequency switching technique with a frequency throw of 10 MHz. The nominal spectral resolution of 38.1 kHz was left unchanged for the final spectra because of the low temperature of this source and, therefore, narrowness of its lines. The average noise at this spectral resolution in the Q band ranges from ∼0.7 mK at 31 GHz to ∼2 mK at 49.5 GHz, which considerably improves previous line surveys in this frequency range for this source (Kaifu et al. 2004).

In order to improve the rotational constants of C_5N^- we used all lines of this species observed with the IRAM 30 m telescope since its detection (Cernicharo et al. 2008). These observations in the λ3 mm band have been described in detail by Cernicharo et al. (2019). They correspond to observations acquired during the last 35 years covering the 70−116 GHz range with very high sensitivity (1−3 mK) over 1 MHz wide channels. Examples of these data can be found in Cernicharo et al. (2004, 2007, 2008, 2019) and Agúndez et al. (2008b, 2014).

The beam size of the Yebes 40 m in the Q band is in the range 36−56″, while that of the IRAM 30 m telescope in the 3 mm domain is 21−30″. Pointing corrections were obtained by observing strong nearby quasars or SiO masers for both sources. Pointing errors were always within 2−3″. The intensity scale for the observations with both telescopes, antenna temperature (T_A^*), was obtained after a calibration procedure that uses two absorbers at different temperatures and the atmospheric transmission model (ATM; Cernicharo 1985; Pardo et al. 2001). Calibration uncertainties are ∼10%. Additional uncertainties could arise, in the case of IRC +10216, from the line intensity fluctuation induced by the time variation of the stellar infrared flux (Cernicharo et al. 2014; Pardo et al. 2018). All data were analyzed via the GILDAS package[2].

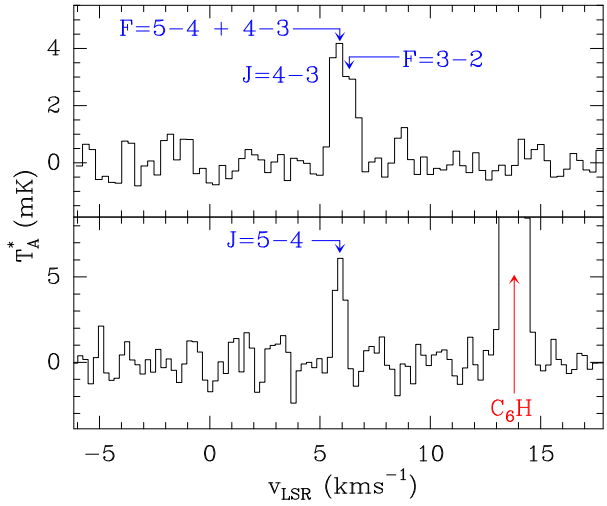

Fig. 1. Lines of C_3N^- observed towards TMC-1 in the 31.0−50.3 GHz frequency range. The abscissa corresponds to the local standard of rest velocity in km s^{-1}. Frequencies and intensities for the observed lines are given in Table 1. The ordinate axis represents the antenna temperature in mK corrected for atmospheric and telescope losses.

3. Results

One of the most remarkable results from the Q-band observations in TMC-1 and IRC +10216 is the presence of a forest of weak lines. Most of these can be assigned to known species and only a few remain unidentified in IRC +10216 (Cernicharo et al. 2019; Pardo et al. 2020) and TMC-1 (Marcelino et al., in prep.). For both sources the level of sensitivity in this work has been increased, as commented previously, by a factor 5−10 with respect to previous works with other telescopes at the same frequencies (Kawaguchi et al. 1995; Kaifu et al. 2004). This high sensitivity has also allowed us to detect all known $C_{2n}H$ and $C_{2n+1}N$ anions in TMC-1. In this Letter we focus on C_3N^- and C_5N^- lines in TMC-1. In addition, we use the observed frequencies of C_5N^- transitions towards IRC +10216 for an improved determination of the rotational and distortion constants of this anion.

3.1. C_3N^-

Laboratory work exists for this anion and frequencies are well determined with accuracies of ≃2 kHz (Thaddeus et al. 2008). This species has two rotational transitions in the 31.0−50.3 GHz frequency range. Figure 1 shows both of these transitions towards TMC-1, while the derived line parameters are given in Table 1. This species was searched towards TMC-1 by Thaddeus et al. (2008) without success, and to the best of our knowledge, this is the first time this anion has been detected in an interstellar cloud.

3.2. C_5N^-

The detected lines of C_5N^- towards TMC-1 are shown in Fig. 2. Only the J = 18−17 transition at 49998.4 MHz has not been

[1] https://nanocosmos.iff.csic.es/

[2] http://www.iram.fr/IRAMFR/GILDAS

Table 1. Observed line parameters for C_3N^- in TMC-1.

Transition	ν_{rest} [a] (MHz)	v_{LSR} (km s^{-1})	Δv [b] (km s^{-1})	$\int T_A^* dv$ [c] (mK km s^{-1})	T_A^* (mK)
$J = 4–3$ $F = 4–3$					
$+F = 5–4$	38812.810	5.82 ± 0.05	0.51 ± 0.13	2.4 ± 0.3	4.5
$J = 4–3$ $F = 3–2$	38812.728	5.84 ± 0.10	0.68 ± 0.16	2.3 ± 0.4	3.3
$J = 5–4$	48515.874	5.90 ± 0.03	0.50 ± 0.07	3.5 ± 0.3	6.5

Notes. [a]Rest frequencies as provided by the MADEX catalogue (Cernicharo 2012). Typical uncertainties are 2 kHz. [b]Line width at half intensity derived by fitting a Gaussian line profile to the observed transitions. [c]Integrated line intensity.

detected. This is, however, justified since the sensitivity of the data at 50 GHz is 3 mK, whereas the expected $J = 18–17$ line intensity is below 5 mK (see also Fig. 2). No C_5N^- lines were detected with the Nobeyama 45 m telescope by Kaifu et al. (2004).

In order to derive precise frequencies for C_5N^- in TMC-1 we fitted, in our Yebes 40 m data, the central v_{LSR} of the line emission from well-known species for which accurate laboratory rotational frequencies exist. From the seven HC_5N rotational transitions in the Q band ($J_{up} = 12$ to $J_{up} = 18$), Cernicharo et al. (in prep.) derive a v_{LSR} of 5.83 ± 0.01 km s^{-1}. From the ^{13}C and ^{15}N isotopologues of HC_5N, they obtain $v_{LSR} = 5.84 \pm 0.01$ km s^{-1}. Hence, we adopt a v_{LSR} of 5.83 km s^{-1} for further frequency determinations in TMC-1. The value given by Kaifu et al. (2004) is 5.85 km s^{-1}, which is practically identical to our result within the uncertainties. Derived line parameters for C_5N^- in TMC-1 are given in Table 2.

The characteristic U-shaped line profiles exhibited by molecular lines in IRC +10216 allow an accurate central frequency determination, within ≃50 kHz (Cernicharo et al. 2018), in spite of the broad emission that covers 29 km s^{-1} (Cernicharo et al. 2000). The v_{LSR} of the source, −26.5 km s^{-1}, has been well determined from the observation of hundreds of lines (Cernicharo et al. 2000). The observed C_5N^- lines in IRC +10216 at $\lambda \sim 7$ mm (Q band) are shown in Fig. A.1. Frequencies and other line parameters are given in Table A.1. This table also includes lines observed in the 3 mm data obtained after the detection of this species in 2008. All lines at 3 mm re-observed after Cernicharo et al. (2008) have a spectral resolution of 0.198 MHz; these lines are shown in Fig. A.2.

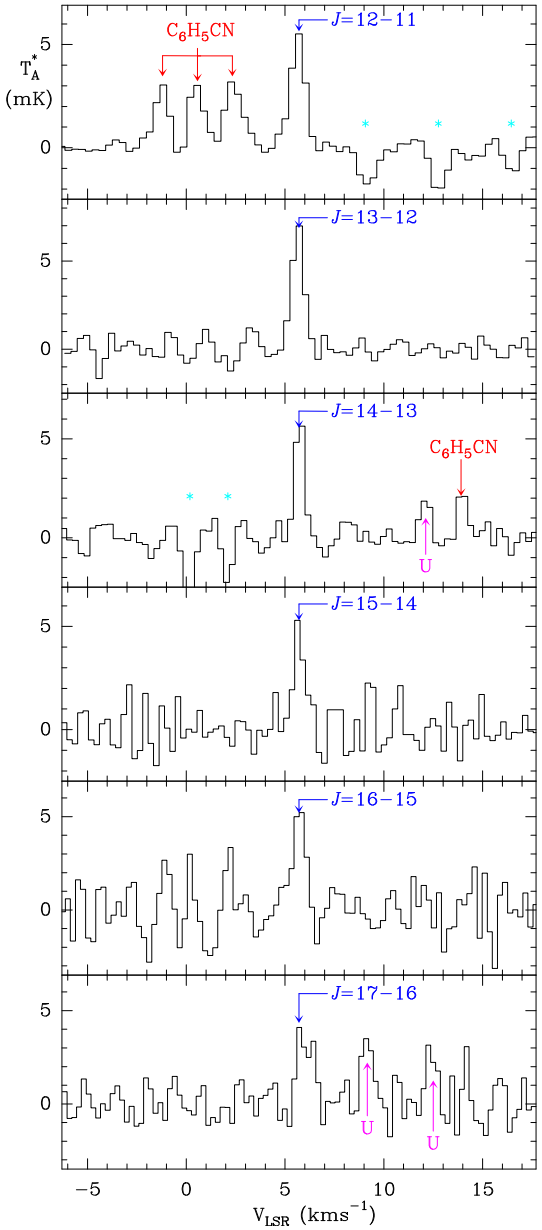

Fig. 2. Same as Fig. 1 but for C_5N^-. Observed frequencies and intensities are given in Table 2.

3.3. New rotational constants for C_5N^-

The frequencies of a linear molecular species can be fitted to this standard expression involving the rotational quantum number J, rotational constant B_0, and the distortion constant D_0:

$$\nu(J \rightarrow J-1) = 2B_0J - 4D_0J^3.$$

Using all observed C_5N^- lines in both sources, the fit provides the following results:

$$B_0 = 1388.86681(19)\ \text{MHz}$$
$$D_0 = 34.44(13) \times 10^{-6}\ \text{MHz},$$

where values between parentheses represent the 1σ uncertainty for the fitted parameters. The data were weighted in the fit according $1/\delta v^2$, where δv is the estimated uncertainty on the observed frequencies. The correlation coefficient between B_0 and D_0 is 0.738 and the standard deviation between the predicted and observed frequencies is 66 kHz. These values significantly improve those derived from previous observations by Cernicharo et al. (2008), $B_0 = 1388.860(2)$ and $D_0 = 33(1) \times 10^{-6}$ MHz. We tried to fit the distortion constant of order six (H_0), but the derived value is only marginally significant. Its inclusion reduces the weighted deviation from 1.03 to 0.89 and the standard deviation from 66 to 53.7 kHz. However, it increases the correlation between the fitted parameters. The derived values in this case, are written as

$$B_0 = 1388.86734(25)\ \text{MHz}$$
$$D_0 = 35.68(44) \times 10^{-6}\ \text{MHz}$$
$$H_0 = 5.0(1.7) \times 10^{-10}\ \text{MHz}.$$

The differences between observed and calculated frequencies are given in Tables 2 and A.1 for TMC-1 and IRC+10216, respectively. New rotational parameters were also derived for C_5N (see Appendix A.1).

Table 2. Observed line parameters for C_5N^- in TMC-1.

J_u	ν_{obs} [a] (MHz)	$\nu_o - \nu_c$ [b] (kHz)	Δv [c] (km s^{-1})	$\int T_A^* dv$ [d] (mK km s^{-1})	T_A^* (mK)
12	33332.572	1.7	0.75 ± 0.08	5.0 ± 0.2	6.2
13	36110.244	5.5	0.73 ± 0.07	5.5 ± 0.2	7.1
14	38887.893	−2.6	0.54 ± 0.09	3.7 ± 0.3	6.4
15	41665.548	7.1	0.50 ± 0.16	2.4 ± 0.4	4.6
16	44443.178	4.5	0.63 ± 0.15	3.3 ± 0.5	4.9
17	47220.754	−38.8	0.76 ± 0.19	2.0 ± 0.5	2.5

Notes. [a]Observed frequencies for a v_{LSR} of 5.83 km s^{-1}. The uncertainty is 10 kHz for all lines except for $J = 17-16$, for which it is 20 kHz. [b]Observed minus calculated frequencies. [c]Line width at half intensity derived by fitting a Gaussian line profile to the observed transitions. [d]Integrated line intensity.

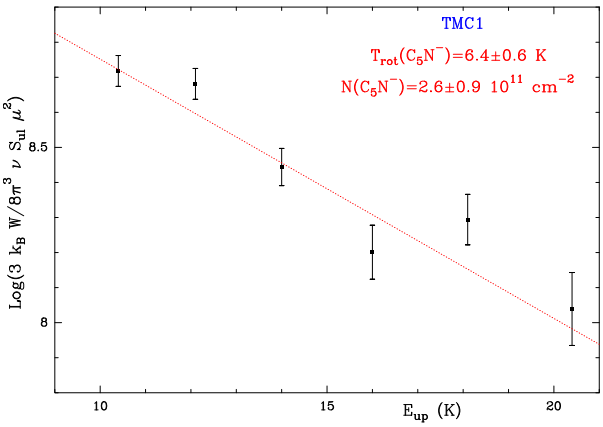

Fig. 3. Rotational diagram for the observed lines of C_5N^- in TMC-1.

4. Discussion

Only two rotational C_3N^- lines have been detected in TMC-1. We assumed a volume density of H_2 of 4×10^4 cm^{-3} (see e.g. Fossé et al. 2001), a kinetic temperature of 10 K, a dipole moment for the molecule of 2.27 D (Pascoli & Lavendy 1999), and the collisional rates of C_3N^-/H_2 from Lara-Moreno et al. (2019). For simulating the source we assumed a circular uniform brightness distribution with a radius of 40″ (see e.g. the intensity maps of different carbon chains presented by Fossé et al. 2001). With this assumed size the source completely covers the main beam of the Yebes 40 m at 50 GHz.

Using the large velocity gradient approximation (LVG) implemented in MADEX (Cernicharo 2012), and correcting the intensities of all observed transitions for the beam efficiency and the source beam dilution, we derive a column density of $N(C_3N^-) = 1.3 \times 10^{11}$ cm^{-2}.

For C_5N^- we have enough observed lines to build the rotational diagram shown in Fig. 3. A dipole moment of 5.2 D was adopted for this species (Botschwina & Oswald 2008). A source size identical to that of C_3N^- was adopted. We derive a rotational temperature of 6.4 ± 0.6 K and a column density of $(2.6 \pm 0.9) \times 10^{11}$ cm^{-2}. We also performed an LVG calculation with MADEX adopting for C_5N^- the collisional rates of C_6H^-/p-H_2 (Walker et al. 2017). For a kinetic temperature of 10 K, the observed intensities corrected for beam efficiency and source beam dilution can be reproduced with a column density of 9×10^{11} cm^{-2}. If the collisional rates of HC_5N/p-H_2 are adopted (F. Lique, priv. comm.), then the column density is 1.5×10^{11} cm^{-2}. Hence, the difference by a factor two of the latter value with respect to that from the rotational diagram is due to the uncertainties on both the collisional rates and the assumed H_2 volume density. We adopt for C_5N^- the column density derived from the rotational diagram of Fig. 3.

The derived line parameters for C_3N and C_5N are given in Tables A.2 and A.3. For C_3N collisional rates are not available and we assumed a rotational temperature of 7 K (that is similar to that of C_5N^-) to compute line intensities assuming local thermodynamical equilibrium conditions (LTE). Assuming the same source size as for the anions, we derive $N(C_3N) = 1.8 \times 10^{13}$ cm^{-2}. For C_5N we can build a rotational diagram based on the data provided in Table A.3, which yields $T_{rot} = 10.1 \pm 1.90$ K and $N(C_5N) = (6.0 \pm 2.5) \times 10^{11}$ cm^{-2}. The adopted dipole moment for this species is 3.385 D (Botschwina 1996). Hence, the $N(C_3N)/N(C_3N^-)$ and $N(C_5N)/N(C_5N^-)$ abundance ratios in TMC-1 are ~140, and ~2.3, respectively.

In IRC +10216 Thaddeus et al. (2008) derived a $N(C_3N)/N(C_3N^-)$ abundance ratio of ≃194, and Cernicharo et al. (2008) obtained a $N(C_5N)/N(C_5N^-)$ abundance ratio around 2. Hence, the observed abundance ratios between neutral radicals C_nN and their anions are very similar in interstellar and circumstellar clouds.

One of the problems in obtaining the C_nN/C_nN^- abundance ratio is the assumed permanent dipole moment for the neutrals. In the case of C_5N, the dipole moment for the ground $^2\Sigma$ electronic state was calculated by Botschwina (1996). However, as discussed by Cernicharo et al. (2008), the C_5N radical has a low lying $^2\Pi$ electronic state with a dipole moment of ~1 D (Pauzat et al. 1991). Detailed calculations by Botschwina (1996) indicate that it lies 500 cm^{-1} above the $^2\Sigma$ ground state. Hence, C_5N could have a dipole moment between these two values in the case of admixing between the $^2\Sigma$ and the $^2\Pi$ states. A dipole moment averaged over both electronic states (i.e., twice as small as that calculated for the unperturbed $^2\Sigma$ state) would raise the C_5N/C_5N^- abundance ratio to ~8 in TMC-1 and IRC +10216, which is very similar to the C_6H/C_6H^- ratio in IRC +10216 (Cernicharo et al. 2007).

The same situation applies to C_4H and C_4H^-. The neutral radical also has a $^2\Sigma^+$ ground electronic state with a first excited $^2\Pi$ electronic state very close in energy. The case has been recently discussed by Oyama et al. (2020) who computed a dipole moment for C_4H 2.4 times larger than the value of the $^2\Sigma^+$ state alone. The effect is a decrease by a factor ~6 on the derived C_4H column densities and an increase of the C_4H/C_4H^- abundance ratio by the same factor.

The chemistry of negative ions in cold interstellar clouds has been discussed by Walsh et al. (2009) and Millar et al. (2017). In the light of the discovery of interstellar C_3N^- and C_5N^-, we revisit the chemistry of these species in this work. We performed a chemical model of a cold dark cloud with typical physical parameters ($T_k = 10$ K, $n_H = 2 \times 10^4$ cm^{-3}, $\zeta = 1.3 \times 10^{-17}$ s^{-1}, $A_V = 30$ mag) and "low metal" elemental abundances (see Agúndez & Wakelam 2013). We adopted the University of Manchester Institute of Science and Technology RATE12 reaction network (McElroy et al. 2013), with a subset of reactions involving HCCN from Loison et al. (2015). According to the model, formation of C_3N^- does not occur via radiative electron attachment to C_3N, which is slow (Petrie & Herbst 1997), but through reactions between N atoms and bare carbon-chain anions C_n^- (with $n \geq 6$), which are rapid and produce several nitrile radical and anions (Eichelberger et al. 2007). In the case of C_5N^-, the reaction of radiative electron attachment to C_5N

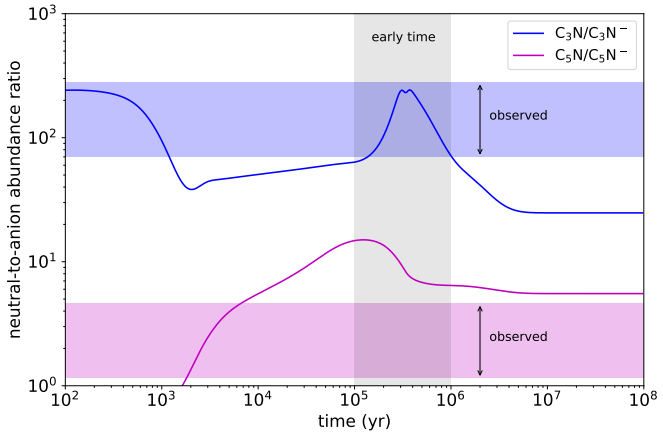

Fig. 4. Neutral-to-anion abundance ratios calculated with the chemical model are shown as a function of time and compared with observed values. The early time (10^5–10^6 yr) at which calculated abundances agree better with observations (see e.g. Agúndez & Wakelam 2013) is indicated. A conservative uncertainty of a factor of 2 is adopted for the observed ratios.

is rapid (Walsh et al. 2009) and dominates the synthesis of this anion. Formation of C_3N^- through dissociative electron attachment to metastable isomers such as HNC_3 (Harada & Herbst 2008) is included and occurs to some extent, although most of C_3N^- is formed by $N + C_n^-$ reactions. Reactions of H^- with HC_3N and HC_5N could be a source of C_3N^- and C_5N^-, although they are likely to be too slow at 10 K based on calculations for similar reactions of H^- with C_2H_2 and C_4H_2 (Gianturco et al. 2016). Destruction of C_3N^- and C_5N^- is dominated by reactions with neutral atoms H, O, and C in cold dark clouds. Nitrile anions have been shown to react rapidly with polar molecules at low temperatures (Joalland et al. 2016). However, it is unlikely that this is a major loss channel for anions in cold dense clouds because, apart from CO, molecules have much lower abundances than neutral atoms.

The much larger rate constant of radiative electron attachment to C_5N compared to C_3N is the main reason why C_5N^- is calculated to be much more abundant with respect to the neutral than C_3N^- (see Fig. 4). The results of our model are similar to the theoretical predictions of Walsh et al. (2009). Calculated neutral-to-anion abundance ratios during the so-called early time (10^5–10^6 yr), at which calculated abundances agree better with observations (see e.g. Agúndez & Wakelam 2013), agree well with the values retrieved from observations for C_3N^-, although they are somewhat higher for C_5N^- (see Fig. 4). We note that, as discussed above, the observed C_5N/C_5N^- ratio could be as high as ~8, in which case model and observations would agree much better. Finally, we point out that the chemical model predicts an abundance of $\sim 3 \times 10^{-11}$ relative to H_2 for CN^-. Adopting a column density of 10^{22} cm^{-2} for H_2 (Cernicharo & Guélin 1987), the predicted column density of CN^- would be 3×10^{11} cm^{-2}, which is below the 3σ upper limit of 1.4×10^{12} cm^{-2} derived by Agúndez et al. (2008a).

This work definitively excludes metal-bearing species, or vibrationally excited states of other known species, as carriers for the series of lines assigned to C_5N^- by Cernicharo et al. (2008), and gives strong support to this identification.

Acknowledgements. We thank Spanish Ministerio de Ciencia e Innovación for funding support through project AYA2016-75066-C2-1-P. We also thank ERC for funding through grant ERC-2013-Syg-610256-NANOCOSMOS. MA and CB thank Ministerio de Ciencia e Innovación for Ramón y Cajal grant RyC-2014-16277 and Juan de la Cierva grant FJCI-2016-27983. We thank support from French National Research Agency through project Anion Cos Chem (ANR-14-CE33-0013). We would like to thank our referee, Prof. S. Yamamoto, for useful comments and suggestions.

References

Agúndez, M., & Wakelam, V. 2013, Chem. Rev., 113, 8710
Agúndez, M., Cernicharo, J., Guélin, M., et al. 2008a, A&A, 478, L19
Agúndez, M., Fonfría, J. P., Cernicharo, J., et al. 2008b, A&A, 479, 493
Agúndez, M., Cernicharo, J., Guélin, M., et al. 2010, A&A, 517, L2
Agúndez, M., Cernicharo, J., & Guélin, M. 2014, A&A, 570, A45
Amano, T. 2008, J. Chem. Phys., 129, 244305
Aoki, K. 2000, Chem. Phys. Lett., 323, 55
Botschwina, P. 1996, Chem. Phys. Lett., 259, 627
Botschwina, P., & Oswald, R. 2008, J. Chem. Phys., 129, 044305
Brünken, S., Gupta, H., Gottlieb, C. A., et al. 2007, ApJ, 664, L43
Cernicharo, J. 1985, Internal IRAM Report (Granada: IRAM)
Cernicharo, J. 2012, in ECLA 2011: Proc. of the European Conference on Laboratory Astrophysics, eds. C. Stehl, C. Joblin, & L. d'Hendecourt (Cambridge: Cambridge Univ. Press), EAS Pub. Ser., 251
Cernicharo, J., & Guélin, M. 1987, A&A, 176, 299
Cernicharo, J., Guélin, M., & Kahane, C. 2000, A&AS, 142, 181
Cernicharo, J., Guélin, M., & Pardo, J. R. 2004, ApJ, 615, L145
Cernicharo, J., Guélin, M., Agúndez, M., et al. 2007, A&A, 467, L37
Cernicharo, J., Guélin, M., Agúndez, M., et al. 2008, ApJ, 688, L83
Cernicharo, J., Teyssier, D., Quintana-Lacaci, G., et al. 2014, ApJ, 796, L21
Cernicharo, J., Guélin, M., Agúndez, M., et al. 2018, A&A, 618, A4
Cernicharo, J., Cabezas, C., Pardo, J. R., et al. 2019, A&A, 630, L2
Cordiner, M. A., Charnley, S. B., Buckle, J. V., et al. 2011, ApJ, 730, L18
Cordiner, M. A., Buckle, J. V., Wirström, E. S., et al. 2013, ApJ, 770, 48
Dalgarno, A., & McCray, R. A. 1973, ApJ, 181, 95
Eichelberger, B., Snow, T. P., Barckholtz, C., & Bierbaum, V. 2007, ApJ, 667, 1283
Fossé, D., Cernicharo, J., Gerin, M., & Cox, P. 2001, ApJ, 552, 168
Gianturco, F. A., Satta, M., Mendolicchio, M., et al. 2016, ApJ, 830, 2
Gottlieb, C. A., Brünken, S., McCarthy, M. C., & Thaddeus, P. 2007, J. Chem. Phys., 126, 191101
Gupta, H., Brünken, S., Tamassia, F., et al. 2007, ApJ, 655, L57
Gupta, H., Gottlieb, C. A., McCarthy, M. C., & Thaddeus, P. 2009, ApJ, 691, 1494
Harada, N., & Herbst, E. 2008, ApJ, 685, 272
Herbst, E. 1981, Nature, 289, 656
Joalland, B., Jamal-Eddine, N., Kłos, J., et al. 2016, J. Phys. Chem. Lett., 7, 2957
Kaifu, N., Ohishi, M., Kawaguchi, K., et al. 2004, PASJ, 56, 69
Kasai, Y., Sumiyoshi, Y., Endo, Y., & Kawaguchi, K. 1997, ApJ, 477, L65
Kawaguchi, K., Kasai, Y., Ishikawa, S., & Kaifu, N. 1995, PASJ, 47, 853
Kawaguchi, K., Fujimori, R., & Aimi, S. 2007, PASJ, 59, L47
Khamesian, M., Douguet, N., Fonseca, S., et al. 2016, Phys. Rev. Lett., 117, 123001
Lara-Moreno, M., Stoecklin, T., & Halvick, P. 2019, MNRAS, 486, 414
Loison, J. C., Hébrard, E., Dobrijevic, M., et al. 2015, Icarus, 247, 218
McCarthy, M. C., Gottlieb, C. A., Gupta, H. C., et al. 2006, ApJ, 652, L141
McElroy, D., Walsh, C., Markwick, A. J., et al. 2013, A&A, 550, A36
Millar, T. J., Walsh, C., & Field, T. A. 2017, Chem. Rev., 117, 1765
Müller, H. S. P., Schlöder, F., Stutzki, J., & Winnewisser, G. 2005, J. Mol. Struct., 742, 215
Pardo, J. R., Cernicharo, J., & Serabyn, E. 2001, IEEE Trans. Antennas Propag., 49, 12
Pardo, J. R., Cernicharo, J., Velilla-Prieto, L., et al. 2018, A&A, 615, L4
Pardo, J. R., Bermúdez, C., Cabezas, C., et al. 2020, A&A, 640, L13
Pascoli, G., & Lavendy, H. 1999, Chem. Phys. Lett., 312, 333
Pauzat, F., Ellinger, Y., & McLean, A. D. 1991, ApJ, 369, L13
Petrie, S., & Herbst, E. 1997, ApJ, 491, 210
Pickett, H. M. 1991, J. Mol. Spectr., 148, 371
Remijan, A. J., Hollis, J. M., Lovas, F. J., et al. 2007, ApJ, 664, L47
Sarre, P. J. 1980, J. Chem. Phys., 77, 769
Sakai, N., Sakai, T., Osamura, T., & Yamamoto, S. 2007, ApJ, 667, L65
Sakai, N., Sakai, T., & Yamamoto, S. 2008, ApJ, 673, L71
Tercero, F., et al. 2020, A&A, submitted
Oyama, T., Ozaki, H., Sumiyoshi, Y., et al. 2020, ApJ, 890, 39
Thaddeus, P., Gottlieb, C. A., Gupta, H., et al. 2008, ApJ, 677, 1132
Walker, K. M., Ligue, F., Dumouchel, F., & Dawes, R. 2017, MNRAS, 466, 831
Walsh, C., Harada, N., Herbst, E., & Millar, T. J. 2009, ApJ, 700, 752

Appendix A: Additional tables and figures

Table A.1. Observed line parameters for C_5N^- in IRC +10216.

J_u	ν_{obs} [a] (MHz)	$\nu_o - \nu_c$ [b] (MHz)	$\int T_A^* dv$ [c] (K km s^{-1})	Notes
12	33332.508 ± 0.050	−0.062	0.063 ± 0.003	
13	36110.197 ± 0.050	−0.040	0.091 ± 0.003	
14	38887.789 ± 0.100	−0.105	0.154 ± 0.005	1
15	41665.527 ± 0.050	−0.013	0.115 ± 0.003	
16	44443.116 ± 0.050	−0.057	0.108 ± 0.003	
17	47220.740 ± 0.050	−0.052	0.102 ± 0.003	
18	49998.450 ± 0.100	+0.052	0.100 ± 0.005	1
26	72218.580 ± 0.050	−0.049	0.303 ± 0.008	
27	74996.039 ± 0.050	−0.032	0.308 ± 0.005	
28	77773.492 ± 0.050	+0.002	0.297 ± 0.004	
29	80550.817 ± 0.050	−0.070	0.264 ± 0.009	
30	83328.258 ± 0.050	−0.003	0.216 ± 0.007	
31				2
32	88882.883 ± 0.050	−0.052	0.233 ± 0.003	
33	91660.297 ± 0.050	+0.063	0.232 ± 0.003	
34	94437.518 ± 0.050	+0.011	0.238 ± 0.003	
35	97214.796 ± 0.050	+0.042	0.216 ± 0.006	
36	99991.999 ± 0.050	+0.026	0.207 ± 0.006	
37	102769.266 ± 0.100	+0.101	0.266 ± 0.007	3
38	105546.319 ± 0.050	−0.008	0.202 ± 0.006	
39	108323.470 ± 0.050	+0.010	0.130 ± 0.003	
40	111100.565 ± 0.100	+0.002	0.111 ± 0.008	
41	113877.556 ± 0.100	−0.081	0.092 ± 0.015	1
48	133316.175 ± 0.150	−0.078	0.056 ± 0.010	4

Notes. [a]Observed frequencies assuming a source v_{LSR} of −26.5 km s^{-1} and an expanding velocity of 14.5 km s^{-1} (Cernicharo et al. 2000, 2018). [b]Observed minus calculated frequencies. [c]Integrated line intensity in K km s^{-1}. [1]Blended with another feature but clear line profile. [2]Fully blended with another spectral feature. Fit not possible. [3]Data smoothed to a resolution of 0.6 MHz. [4]Data smoothed to a resolution of 1.0 MHz.

Line parameters for C_5N^- towards IRC +10216 are given in Table A.1. The observed lines are shown in Figs. A.1 and A.2. The data in the 3 mm domain (see Fig. A.2) considerably improve the signal to noise ratio of the lines reported by Cernicharo et al. (2008). The new rotational constants derived from these frequencies and those of TMC-1 are discussed in Sect. 3.3.

The observed line parameters for C_3N and C_5N in TMC-1, which are needed to compute the column density of these species and to compare with that of their anions, are given in Tables A.2 and A.3. For C_3N, accurate frequency predictions can be found in the Cologne Database for Molecular Spectroscopy (CDMS; Müller et al. 2005). However, we discuss below the case of C_5N, as significant deviations between predicted and measured frequencies in space are observed.

A.1. New rotational parameters for C_5N

For C_5N the frequencies of rotational lines up to $J = 6$ ($\nu_{max} = 16.842$ GHz) were measured in the laboratory by Kasai et al. (1997). These authors provide frequency predictions up to 98.2 GHz that are systematically below the observed frequencies of this species towards TMC-1 (data provided in Table A.3) and IRC +10216 (data provided in Table A.4). In order to derive more accurate predictions we fitted the observed astronomical

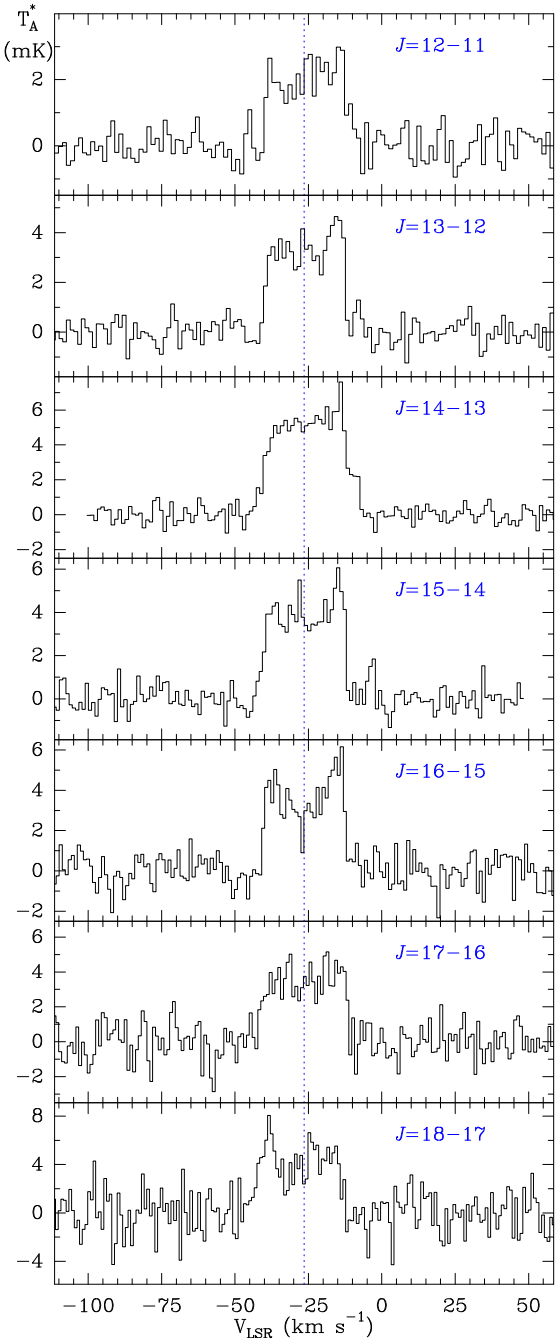

Fig. A.1. Rotational transitions of C_5N^- observed towards IRC +10216 in the 31−50 GHz range. Derived frequencies and intensities are given in Table A.1. Figure A.2 shows the lines of the same species observed with the IRAM 30 m telescope at $\lambda = 3$ mm.

frequencies to the same Hamiltonian than Kasai et al. (1997). The fits only consider frequencies measured in astronomical (space) sources that have an unresolved hyperfine structure and a merged set of space and laboratory frequencies. The results are provided in Table A.5. The poorly determined distortion constant from the laboratory data alone is responsible for the observed discrepancies. The new D value derived from space data alone is 44.2 ± 0.2 Hz, compared with the laboratory value of 50 ± 10 Hz. In IRC +10216 several additional doublets of C_5N are detected between $J_{up} = 40$ to $J_{up} = 48$. However, their line intensity is weak and the derived frequencies have uncertainties of ∼1 MHz. These have not been included in the fit.

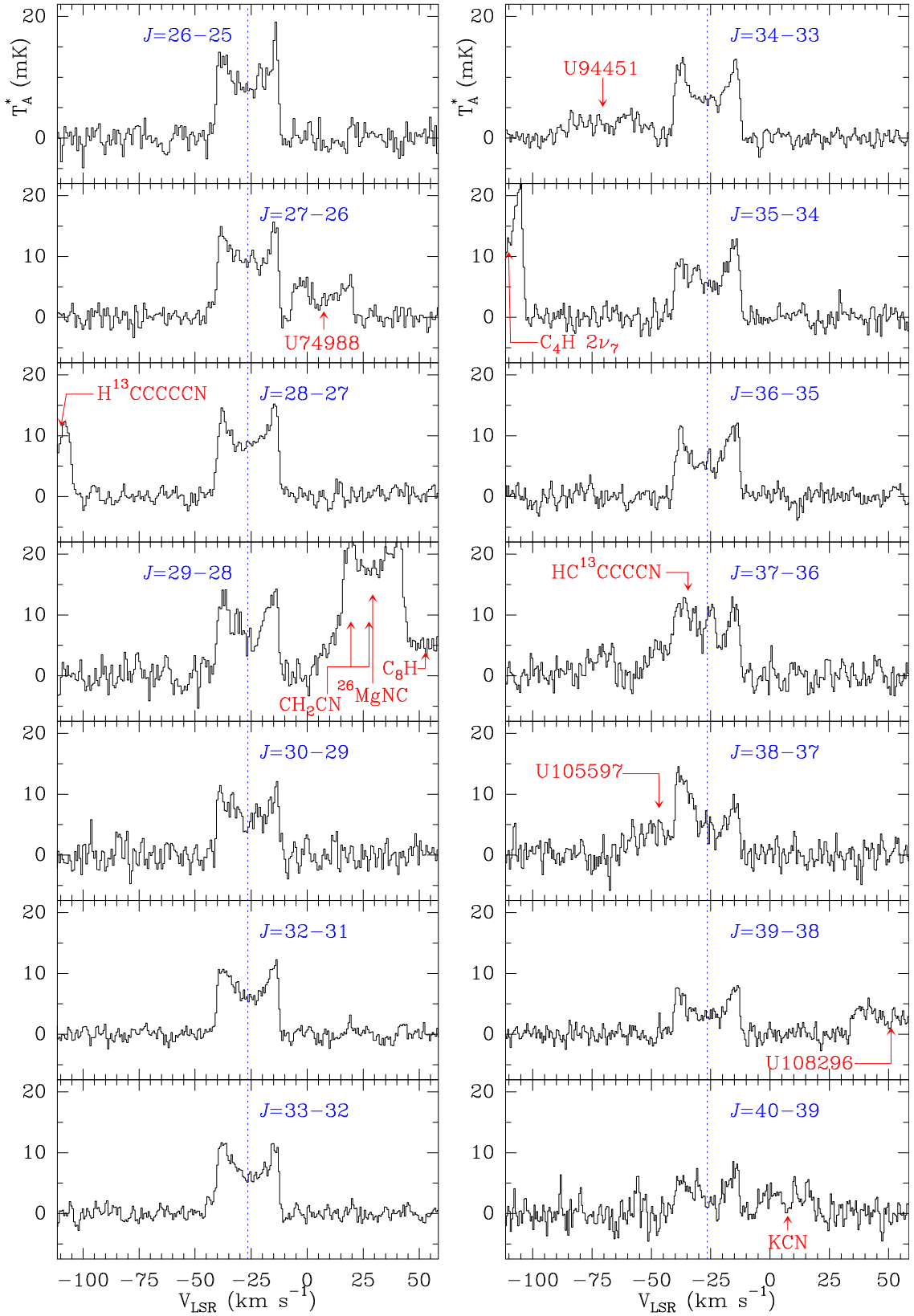

Fig. A.2. Observed lines of C_5N^- towards IRC +10216 in the 3 mm domain with the IRAM 30 m telescope. Spectral resolution is 0.19 MHz for all lines. The abscissa corresponds to the local standard of rest velocity in km s^{-1}. Frequencies and intensities for the observed lines are given in Table A.1. The ordinate is the antenna temperature corrected for atmospheric and telescope losses in mK.

In addition we combined in one fit all the rotational transitions measured so far for C_5N, including those from laboratory measurements and those observed in TMC-1 and IRC +10216. We used the SPFIT program (Pickett 1991). The results are shown in Table A.5. In all these fits the data were weighted according $1/\sigma^2$, where σ is the estimated uncertainty on the

Table A.2. Observed line parameters for C_3N in TMC-1.

$N_u\ J_u\ F_u \rightarrow N_l\ J_l\ F_l$	$\nu_{\rm rest}$ [a] (MHz)	$v_{\rm LSR}$ (km s^{-1})	$\int T_{\rm A}^* {\rm d}v$ [b] (mK km s^{-1})	Δv [c] (km s^{-1})	$T_{\rm A}^*$ (mK)
4 4.5 4.5→3 3.5 4.5	39571.110 ± 0.027	5.78 ± 0.02	5.7 ± 1.0	0.61 ± 0.05	8.8
4 4.5 3.5→3 3.5 2.5	39571.319 ± 0.003	5.72 ± 0.01	136.7 ± 1.0	0.56 ± 0.01	230.6
4 4.5 4.5→3 3.5 3.5	39571.326 ± 0.003 [e]				
4 4.5 5.5→3 3.5 4.5	39571.397 ± 0.003	5.73 ± 0.01	160.0 ± 3.0	0.51 ± 0.02	297.2
4 4.5 3.5→3 3.5 3.5	39574.032 ± 0.044	5.61 ± 0.02	6.0 ± 1.0	0.53 ± 0.04	10.7
4 3.5 3.5→3 2.5 3.5	39587.553 ± 0.048	5.86 ± 0.03	7.8 ± 1.0	0.59 ± 0.04	12.3
4 3.5 2.5→3 2.5 1.5	39590.129 ± 0.004	5.73 ± 0.01	45.4 ± 1.0	0.36 ± 0.01	119.3
4 3.5 3.5→3 2.5 2.5	39590.204 ± 0.004	5.70 ± 0.01	179.5 ± 3.0	0.56 ± 0.01	301.2
4 3.5 4.5→3 2.5 3.5	39590.212 ± 0.004 [e]				
4 3.5 2.5→3 2.5 2.5	39591.004 ± 0.028	5.62 ± 0.02	7.6 ± 1.0	0.58 ± 0.05	12.4
5 5.5 →4 4.5 [d]	49466.424 ± 0.003	5.70 ± 0.02	201.4 ± 3.0	0.66 ± 0.04	286.9
5 4.5 →4 3.5 [d]	49485.227 ± 0.005	5.67 ± 0.02	164.8 ± 3.0	0.64 ± 0.04	242.1

Notes. [a]Rest frequency from the CDMS catalogue (Müller et al. 2005). [b]Integrated line intensity in K ± km s^{-1}. [c]Line width at half intensity derived by fitting a Gaussian line profile to the observed transitions (in km s^{-1}). [d]Unresolved hyperfine structure. Rest frequencies correspond to the weighted value of the three stronger components. [e]Two hyperfine components are unresolved. Rest frequencies correspond to the weighted value of these two components.

Table A.3. Observed line parameters for C_5N in TMC-1.

$N_u\ J_u$	$\nu_{\rm obs}$ [a] (MHz)	$\int T_{\rm A}^* {\rm d}v$ [b] (mK km s^{-1})	Δv [c] (km s^{-1})	$T_{\rm A}^*$ (mK)
12 12.5	33668.248	7.4 ± 0.5	0.80 ± 0.04	8.8
12 11.5	33678.986	6.6 ± 0.5	0.85 ± 0.05	7.4
13 13.5	36474.328	6.3 ± 0.7	0.65 ± 0.31	9.1
13 12.5	36485.068	4.3 ± 0.6	0.52 ± 0.05	7.7
14 14.5	39280.400	5.8 ± 0.6	0.55 ± 0.05	9.9
14 13.5	39291.136	5.1 ± 0.8	0.62 ± 0.07	7.8
15 15.5	42086.452	3.6 ± 0.9	0.44 ± 0.07	7.8
15 14.5	42097.179	2.9 ± 1.0	0.46 ± 0.08	6.0
16 16.5	44892.479	3.7 ± 1.0	0.64 ± 0.14	5.4
16 15.5	44903.223	3.5 ± 1.0	0.39 ± 0.10	8.4
17 17.5	47698.500	4.1 ± 1.1	0.48 ± 0.13	8.2
17 16.5	47709.233	7.5 ± 1.1	0.78 ± 0.12	9.0

Notes. [a]Observed frequency in MHz assuming a $v_{\rm LSR}$ of 5.83 km s^{-1}. Frequency uncertainty is 10 kHz for all lines. [b]Integrated line intensity in K km s^{-1}. [c]Line width at half intensity derived by fitting a Gaussian line profile to the observed transitions (in km s^{-1}).

measured frequencies. We obtained new values for the rotational and centrifugal distortion constants for the three spin-rotation constants and also for the nuclear quadruple coupling constant. In total we analyzed 69 rotational transitions. We tried to determine additional parameters such as the distortion constant H or the spin-rotation constant γ_D, but the attempts resulted to be unfruitful. The uncertainty in the rotational constant, B, improves from 0.54 kHz at Kasai et al. (1997) to 0.15 kHz. The most significant change corresponds to the distortion constant, which has an uncertainty of 10 Hz from the laboratory data alone, and 0.3 Hz when the lines from TMC-1 and IRC +10216 are included.

The fit to the TMC-1 and IRC +10216 alone allows us to predict frequencies without hyperfine splitting with an accuracy better than 0.1 MHz up to $N_{\rm up} = 55$ ($\nu \sim 154.3$ GHz). Observable hyperfine splitting in TMC-1 could occur for transitions with $N \leq 8$ ($\nu \sim 22.4$ GHz). In this case, the merged fit to the laboratory and space data is recommended to compute the expected frequencies.

Table A.4. Observed line parameters for C_5N in IRC +10216.

$N_u\ J_u$	$\nu_{\rm obs}$ [a] (MHz)	$\int T_{\rm A}^* {\rm d}v$ [b] (mK km s^{-1})	Notes
26 26.5	72951.721 ± 0.050	18 ± 6	1,A
26 25.5	.....	.....	2
27 27.5	75757.571 ± 0.050	23 ± 3	A
27 26.5	75768.214 ± 0.100	29 ± 5	1,B
28 28.5	78563.437 ± 0.100	18 ± 3	B
28 27.5	78573.910 ± 0.100	19 ± 3	B
29 29.5	81368.856 ± 0.150	32 ± 2	C
29 28.5	81379.846 ± 0.150	28 ± 2	C
30 30.5	84174.795 ± 0.200	31 ± 6	C
30 29.5	.....	.....	2
31 31.5	86980.324 ± 0.150	25 ± 3	C
31 30.5	.....	.....	2,C
32 32.5	89785.932 ± 0.150	27 ± 1	C
32 31.5	89796.811 ± 0.150	33 ± 2	C
33 33.5	92591.638 ± 0.150	24 ± 1	C
33 32.5	92602.409 ± 0.150	29 ± 1	C
34 34.5	95397.144 ± 0.200	43 ± 7	1,C
34 33.5	.....	.....	2
35 35.5	98202.488 ±0.150	24 ± 3	C
35 34.5	98213.325 ±0.200	15 ± 5	1,C
36 36.5	101008.060 ±0.150	30 ± 3	C
36 35.5	101018.872 ±0.150	26 ± 3	C
37 37.5	103813.438 ±0.150	32 ± 4	C
37 36.5	103824.263 ±0.150	32 ± 4	1,C
38 38.5	106618.712 ±0.200	46 ± 4	C
38 37.5	106629.939 ±0.200	29 ± 4	C
39 39.5	.....	.....	2
39 38.5	.....	.....	2
40 40.5	112229.929 ± 0.500	25 ± 5	C
40 39.5	112240.834 ± 0.500	28 ± 6	C

Notes. [a]Observed frequency assuming a $v_{\rm LSR}$ of −26.5 km s^{-1} (Cernicharo et al. 2000, 2018). [b]Integrated line intensity in mK km s^{-1}. Expanding velocity fixed to 14.5 km s^{-1} (Cernicharo et al. 2000, 2018). [(1)]Partially blended with another spectral feature. Fit still possible. [(2)]Fully blended with another stronger feature. Unreliable fit. [(A)]Spectral resolution of 0.2 MHz. [(B)]Spectral resolution of 0.6 MHz. [(C)]Spectral resolution of 1.0 MHz.

Table A.5. New derived rotational parameters for C_5N from TMC-1 & IRC +10216.

Constant [a]	Lab [b]	TMC-1 [c]	TMC-1 & IRC +10216 [d]	Space + Lab [e]
B	1403.07981(54)	1403.07995(19)	1403.08041(13)	1403.07974(15)
D	0.000050(10)	0.00004324(41)	0.00004423(20)	0.00004354(30)
γ	−10.7472(35)	−10.7363(23)	−10.7360(44)	−10.7478(27)
b	1.583(13)	.....	.....	1.5810(94)
c	−3.613(25)	.....	.....	−3.615(18)
eQq	−4.341(17)	.....	.....	−4.342(13)
N_{max} [f]	6	17	40	40
σ(kHz) [g]	10	4.1	122	96

Notes. [a]Rotational constants in MHz. [b]Laboratory rotational parameters from Kasai et al. (1997). [c]Rotational parameters derived from the observed line frequencies in TMC-1 (see Table A.3). [d]Rotational parameters derived from the observed line frequencies in TMC-1 (see Table A.3) and IRC +10216 (see Table A.4). [e]Merged fit to the laboratory and the TMC-1 and IRC +10216 data. [f]Highest rotational quantum number observed. [g]Standard deviation of the fit in kHz.